eLife

Reviewed Preprint
v3 • July 31, 2024
Revised by authors

Reviewed Preprint
v2 • April 26, 2024

Reviewed Preprint
v1 • November 7, 2023

Medicine

PKR activation-induced mitochondrial dysfunction in HIV-transgenic mice with nephropathy

Teruhiko Yoshida, Khun Zaw Latt, Avi Z Rosenberg, Briana A Santo, Komuraiah Myakala, Yu Ishimoto, Yongmei Zhao, Shashi Shrivastav, Bryce A Jones, Xiaoping Yang, Xiaoxin X Wang, Vincent M Tutino, Pinaki Sarder, Moshe Levi, Koji Okamoto, Cheryl A Winkler, Jeffrey B Kopp

Kidney Disease Section, Kidney Diseases Branch, NIDDK, NIH, Bethesda, MD • Department of Pathology, Johns Hopkins Medical Institutions, Baltimore, MD • Department of Pathology and Anatomical Sciences, Jacobs School of Medicine & Biomedical Sciences, University at Buffalo, Buffalo, NY • Department of Biochemistry and Molecular & Cellular Biology, Georgetown University, Washington, DC • Polycystic Kidney Disease Section, Kidney Diseases Branch, NIDDK, NIH, Bethesda, MD • Frederick National Laboratory for Cancer Research, NCI, NIH, Frederick, MD • College of Medicine, University of Florida, Gainesville, FL • Nephrology Endocrinology and Vascular Medicine, Tohoku University Hospital, Sendai, Japan

Abstract

HIV disease remains prevalent in the USA and chronic kidney disease remains a major cause of morbidity in HIV-1-positive patients. Host double-stranded RNA (dsRNA)-activated protein kinase (PKR) is a sensor for viral dsRNA, including HIV-1. We show that PKR inhibition by compound C16 ameliorates the HIV-associated nephropathy (HIVAN) kidney phenotype in the Tg26 transgenic mouse model, with reversal of mitochondrial dysfunction. Combined analysis of single-nucleus RNA-seq and bulk RNA-seq data revealed that oxidative phosphorylation was one of the most downregulated pathways and identified signal transducer and activator of transcription (STAT3) as a potential mediating factor. We identified in Tg26 mice a novel proximal tubular cell cluster enriched in mitochondrial transcripts. Podocytes showed high levels of HIV-1 gene expression and dysregulation of cytoskeleton-related genes; and these cells dedifferentiated. In injured proximal tubules, cell-cell interaction analysis indicated activation of the profibrogenic PKR-STAT3-platelet derived growth factor (PDGF)-D pathway. These findings suggest that PKR inhibition and mitochondrial rescue are potential novel therapeutic approaches for HIVAN.

Translational Statement

This work identified mitochondrial dysfunction in transgenic mice manifesting HIV-associated nephropathy mice kidney, using combination of single-nuclear and bulk RNA-seq analysis. Kidney damage was ameliorated by the PKR inhibitor C16, and mitochondrial rescue was shown by transcriptomic profiling and functional assay. These findings suggest that PKR inhibition and mitochondrial rescue are potential therapeutic approaches for HIV-associated nephropathy.

eLife assessment

This study presents **valuable** new insights into a HIV-associated nephropathy (HIVAN) kidney phenotype in the Tg26 transgenic mouse model, and delineates the kidney cell types that express HIV genes and are injured in these HIV-transgenic mice. A series of **compelling** experiments demonstrated that PKR inhibition can ameliorate HIVAN with reversal of mitochondrial dysfunction (mainly confined to endothelial cells), a prominent feature shared in other kidney diseases. The data support that inhibition of PKR and mitochondrial dysfunction has potential clinical significance for HIVAN.

https://doi.org/10.7554/eLife.91260.3.sa3

Introduction

The World Health Organization (WHO) reported that in 2020, ~1.5 million people became newly HIV positive, ~37 million people were living with HIV, and ~680,000 people globally died from HIV-related causes.[1] HIV remains prevalent in the USA[2] and even more highly prevalent in sub-Saharan Africa, especially in East and Southern Africa.[3] Chronic kidney disease (CKD) remains a major co-morbidity in HIV positive individuals, even with availability of combined anti-retroviral therapy.[4] The most severe form of CKD in persons with untreated or undertreated HIV infection is HIV-nephropathy (HIVAN), collapsing glomerulopathy. Therapy for HIVAN includes combined anti-retroviral therapy, coupled with renin-angiotensin-aldosterone system blockade, to prevent CKD progression.[5,6]

The Tg26 transgenic is a widely-used HIVAN model. The HIV-1 transgene expresses in kidney cells and the model manifests histological features similar to those of human HIVAN, including collapsing glomerulopathy, microtubular dilatation and interstitial fibrosis.[7] The mice develop progressive renal dysfunction and progress to terminal uremia.[8,9]

Diverse therapeutic approaches are effective in Tg26 kidney disease, including inhibitors of mammalian target of rapamycin (mTOR),[10–12] Notch inhibition,[13,14] renin-angiotensin system inhibition,[15,16] cyclin-dependent kinase inhibition,[17] sirtuin1 agonist or overexpression,[18] STAT3 activation reduction,[19,20] retinoic acid receptor agonist,[21] and NF-kB inhibition.[22] Recent reports have identified several injury pathways, including NLRP3[23] and mitochondrial dysfunction.[24,25] Bulk multi-omics approaches using mRNA microarrays and protein-DNA arrays[26] identified homeo-domain interacting protein kinase-2 (HIPK2) as a regulator of Tg26 renal pathology; this was confirmed in recent reports.[27,28] A mRNA microarray approach characterized bulk transcriptional profiles during progressive renal disease.[29] While these reports have provided novel insights into tissue transcriptional dynamics, studies have not been performed at single-cell or single-nucleus resolution.

Double-stranded RNA (dsRNA)-activated protein kinase (PKR) is a sensor for dsRNA and is activated in response to viral infections, including HIV-1. In the US and globally, HIV remains an important problem that disproportionately affects marginalized groups, including the Black/African-American community.[1] *APOL1* risk variants, exclusively present in individuals with recent sub-Saharan ancestry, damage podocytes through various mechanisms including PKR activation by *APOL1* mRNA.[30] The PKR-inhibiting oxoindole/imidazole compound C16 is beneficial in neuroinflammatory disease models.[31,32]

We hypothesized that PKR activation is a mechanistic pathway shared by HIV- and APOL1-mediated nephropathies, considering the high odds ratio for HIVAN among African Americans (OR 29) and South Africans (OR 89) carrying two *APOL1* risk alleles.[33] We investigated the effects of PKR inhibition in the Tg26 HIVAN mouse model, which expresses HIV regulatory and accessory genes. We used single-nucleus and bulk RNA-sequencing methods to identify transcriptional changes between study groups and to uncover associated molecular mechanisms in an unbiased fashion.

Methods

Mice

Hemizygous ($Tg26^{+/-}$) male mice were bred with wild type FVB/N female mice to generate Tg26 hemizygous mice. Transgenic mice were identified by PCR genotyping. We studied both male and female mice, aged 6–12 weeks. Mice in treatment groups were matched for sex.

For PKR inhibition treatment, the C16 treatment group mice received 10 µg/kg body weight of C16 (Sigma-Aldrich, St. Louis, MO) dissolved in 0.5% DMSO-PBS (10 ml/kg body weight), administered intraperitoneally three times weekly[30] from 6 weeks to 12 weeks of age. Urine collection (in 24-hour metabolic cages) and body weight measurements were performed at 6 weeks of age before treatment and 12 weeks of age after treatment. Mice were euthanized and plasma, serum and kidney samples were collected at age of 12 weeks.

Mouse kidney pathological evaluation, In situ hybridization (ISH) and Immunohistochemistry

Mouse kidney tissues were fixed with 10% buffered formalin for 24 hours, embedded in paraffin, and sectioned at 4-5 µm, and stained with hematoxylin and eosin, periodic acid Schiff, and picrosirius red. Chromogenic *in situ* detection of RNA was performed using RNAscope 2.5 HD Reagent Kit (catalog # 322310, Advanced Cell Diagnostics, Biotechne, Minneapolis, MN) with the RNA probes Mm-mt-Co1, Mm-mt-Atp6, dabB (negative control), Mm-Ppib (positive control) (catalog # 517121, 544401, 310043, 313911).

For immunohistochemistry, tissue sections were deparaffinized/rehydrated, antigens were retrieved by citrate buffer, and non-specific binding was blocked. Sections were incubated with primary antibody against phospho-Stat3 (Tyr705) (#9145, 1:100 dilution, Cell Signaling, Danvers, MA), phopho-PKR (Thr 446) (#sc16565, 1:50 dilution, Santa Cruz Biotechnology, Dallas, TX) and platelet-derived growth factor (PDGF)-D (ab181845, Abcam, 1:100 dilution, Cambridge, UK). Detailed methods including estimation of glomerular podocyte count by PodoCount[34] are described in the Supplemental Methods.

Immunoblotting

Tissues were lysed in a radioimmunopreciptation assay (RIPA) buffer (Thermo Fisher Scientific, Waltham, MA) containing a protease inhibitor/ phosphatase inhibitor cocktail (#78440, Thermo Fisher Scientific). Lysates were separated by SDS-polyacrylamide gel electrophoresis (SDS-PAGE) (gradient gel 4-12%, MOPS buffer) and the proteins subjected to Western blotting and blocked for one hour in Odyssey blocking buffer (LI-COR, Lincoln, NE). Blots were incubated following the iBind protocol (Thermo Fisher Scientific). Primary antibodies were Phospho-Stat3 (Tyr705) (#9145, 1:2000 dilution, Cell Signaling, Danvers, MA), Stat3 (#9139, 1:1000 dilution, Cell Signaling), β-actin (#47778, 1:5000 dilution, Santa Cruz Biotechnology), Total OXPHOS Rodent (#ab110413, 1:250 dilution, Abcam, Cambridge, UK), VDAC (# 4661, 1:1000 dilution, Cell Signaling). Blots were imaged using the Odyssey infrared scanner (LI-COR, Lincoln, NE).

Bulk RNA-sequencing

Mouse kidney outer cortex tissues were dissected and homogenized in QIAzol (QIAGEN, Germantown, MD). Total RNA samples were extracted using RNeasy Plus Universal Kit (QIAGEN) following the manufacturer's protocol including removal of genomic DNA step. RNA samples were pooled and sequenced on NovaSeq6000 S1 flowcell using Illumina TruSeq Stranded mRNA Library Prep and paired-end sequencing with read length 101bps (2×101 cycles). The samples had 46 to 72 million pass filter reads and more than 92% of bases calls were above a quality score of Q30. Sample reads were trimmed for adapters and low-quality bases using Cutadapt[35]. The trimmed reads were mapped to a reference genome (Mouse - mm10). Transcripts were annotated by Ensembl v96 using STAR aligner. Gene expression quantification analysis was performed for all samples using STAR/RSEM tools. DESeq2[36] was used for differential expression analysis from raw count data and normalized data were used for Gene set enrichment analysis (GSEA v4.1.0).[37,38] Pathway analysis including upstream regulator analyses were generated using QIAGEN Ingenuity Pathway Analysis.[39]

Single-nucleus RNA-sequencing

Nuclei from frozen mouse kidney outer cortex tissue samples and glomeruli-enriched samples were prepared at 4°C.[40] Tissue fragments (~ 8 mm^3) were cut by razor blades in EZlysis buffer (#NUC101-1KT, Sigma-Aldrich) and homogenized 30 times using a loose Dounce homogenizer and 5 times by tight pestle. After 5 min of incubation, homogenates were passed through 40 µm filters (PluriSelect, El Cajon, CA) and centrifuged at 500g at 4°C for 5 min. Pellets were washed with EZlysis buffer and again centrifuged at 500g at 4°C for 5 min. Pellets were resuspended in DPBS with 1% FBS and passed through 5 µm filters (PluriSelect) to make final nuclei preparations for loading on to 10xChromium Chip G (10x Genomics, Pleasanton, CA) and formation of gel beads in emulsion (GEM).

Single nuclear isolation, RNA capture, cDNA preparation, and library preparation were accomplished following the manufacturer's protocol (Chromium Next GEM Single Cell 3' Reagent Kit, v3.1 chemistry, 10x Genomics). Prepared cDNA libraries were sequenced. Analysis was performed with the Cell Ranger software using the default parameters with pre-mRNA analysis turned on. The reference was built from mm10 reference genome complemented with HIV-1 viral sequences.

Single-nucleus RNA-seq Analysis

SoupX (version 1.5.2)[41] was used to remove ambient RNA, following the default protocol by "autoEstCont" and "adjustCounts" functions. Doublets were identified and removed by DoubletFinder (version 2.0.3)[42]. Nuclei were filtered out that met any of the following criteria: detected genes < 200 or > 4000, total RNA count > 15000, or mitochondrial transcripts > 20%. Integration of single-nucleus gene expression data was performed using Seurat (version 4.0.5).[43] After filtering, 57,061 cells remained. Clustering of the combined data used the first 30 principal components at a resolution of 0.6 and identified 25 distinct cell clusters. After removal of 2 doublet clusters, 56,976 cells from 23 clusters were used for downstream analysis. Cell type identification was done based on the expression levels of known marker genes. Pseudotime analysis of podocytes and proximal tubule cells was performed by using the R package Monocle 3 (version 1.0)[44], considering wild-type cells as the root state. Cell-cell interaction analysis was performed using CellChat (version 1.5.0).[45] Pathway analysis including upstream regulator analysis were accomplished through the use of QIAGEN Ingenuity Pathway Analysis.[39]

Seahorse Extracellular Flux Assay

Seahorse 96-well assay plates (Agilent, Santa Clara, CA) were pre-coated twice with 20 µl/well of 0.01% poly-L-lysine solution (P4707, Sigma-Aldrich) and washed twice with PBS, 200 µl/well. Glomerular and proximal tubular samples were plated in EGM-2 medium (CC-3162, Lonza, Walkersville, MD) and placed in a CO_2-incubator for 30 minutes for the attachment.

Seahorse Mito Stress Tests were conducted as described.[30] Data were normalized by total nucleic acid content measured by CyQUANT Cell Proliferation (C7026, Thermo Fisher Scientific) and analyzed by Wave 2.6.1 (Agilent). Detailed method is described in the Supplemental Methods.

Study Approval

Mouse experiments were conducted in accordance with the NIH Guide for the Care and Use of Laboratory Animals and were approved in advance by the NIDDK Animal Care and Use Committee (Animal study proposals, K097-KDB-17 & K096-KDB-20).

Results

PKR inhibition ameliorates kidney injury in Tg26 mice

The trans-activating regions (TAR) RNA in the HIV-1 long terminal repeats (LTRs) at the 5' and 3' ends of the HIV genome form double stranded RNA (dsRNA) structures and induce PKR autophosphorylation, thereby activating PKR.[46] As PKR is a potent driver of many stress response pathways, including translational shutdown, apoptosis, inflammation and metabolism, we hypothesized that PKR inhibition by the PKR-specific oxoindole/imidazole inhibitor C16 might rescue kidney injury in Tg26 mice. We administered C16 to Tg26 and wild-type mice from 6 to 12 weeks of age, and we evaluated the kidney phenotype. C16-treated Tg26 mice had lower serum creatinine (**Figure 1A**), reduced albuminuria (**Figure 1B, 1C**) and reduced pPKR abundance (**Supplemental Figure 1A-D**) compared to control Tg26 mice. Further, C16 treatment reduced urinary excretion of the kidney injury marker neutrophil gelatinase-associated lipocalin (NGAL) (**Figure 1D**).

At 12 weeks of age, there was less glomerulosclerosis and of microtubular dilatation in C16-treated Tg26 mice (**Figure 1E-G**). Histomorphologic quantification confirmed that C16 treatment reduced glomerular injury, assessed as segmental glomerulosclerosis and global glomerulosclerosis (**Figure 1H, 1I**), and as fibrosis extent, quantified by picrosirius red staining (**Figure 1J-M**).

Combination of single-nucleus RNA-seq and bulk RNA-seq to profile transcriptomic changes in Tg26 mice

To investigate molecular mechanisms in Tg26 kidney and the effect of PKR inhibition, we conducted bulk RNA-seq of kidney cortex from the four groups (WT, WT treated with C16, Tg26, and Tg26 treated with C16; n=3 each) and single-nucleus RNA-seq of kidney cortex from six samples (WT, Tg26, and Tg26 treated with C16; n=2 each) and of two samples of glomeruli (WT and Tg26; n=1 each) to enrich for glomerular cells (**Figure 2A**). Bulk RNA-seq data clustered well by treatment groups in a principal component analysis plot (**Figure 2B**). Single-nucleus RNA-seq profiled 56,976 nuclei. We identified 23 cell clusters, including a novel cell type (PT-Mito, proximal tubule cell cluster with a higher expression level of mitochondrial genes compared to adjacent cells), as shown as a uniform manifold approximation and projection (UMAP) plot (**Figure 2C**, **Supplemental Figure 2C**). Marker genes for each cluster used for annotation are shown in **Figure 2D**. Taking advantage of unbiased clustering in single-nucleus RNA-seq, we tabulated cell

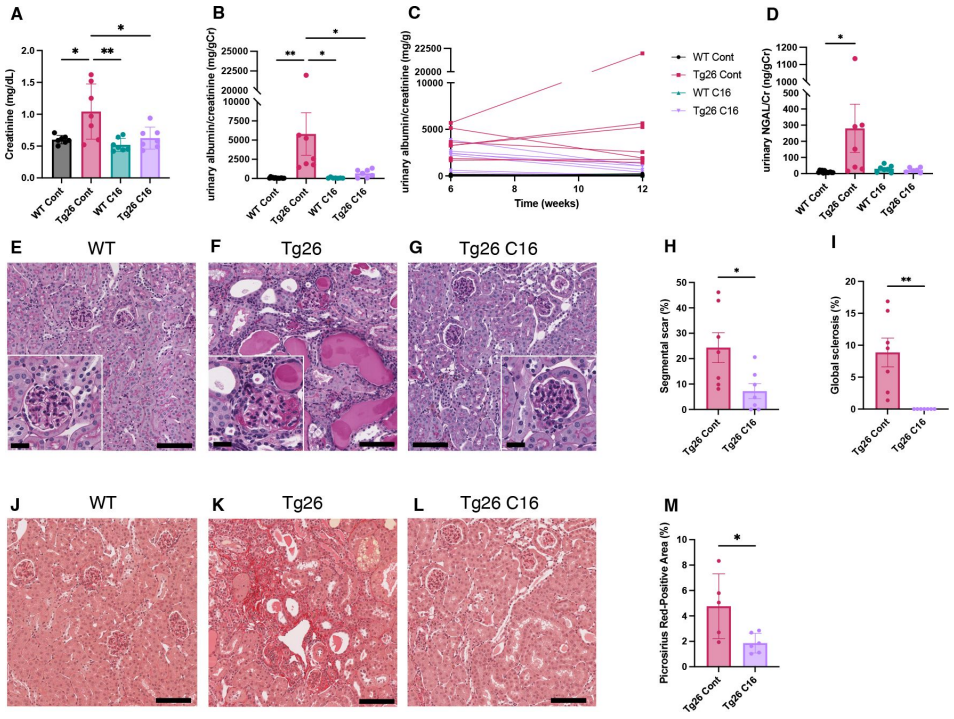

Figure. 1

PKR inhibition by C16 ameliorates Tg26 mice kidney phenotype.

(**A-D**) Shown are the following: plasma creatinine (mg/dL), urinary albumin-to-creatinine ratio (mg/g creatinine), urinary albumin-to-creatinine ratio (mg/g creatinine) of 6 and 12 weeks of age, urinary NGAL-to-creatinine ratio (ng/g creatinine). (**E-G**) Representative PAS staining images of WT, Tg26 and C16 treated Tg26 kidney. (**H, I**) Quantitative analysis of glomeruli for segmental scarring and global sclerosis. (**J-L**) Representative Picrosirius Red-staining images of WT, Tg26 and C16 treated Tg26 kidney. (**M**) Quantitative analysis of Picrosirius Red-staining area. (One-way ANOVA (**A, B, D**), t-test (**H, I, M**); *, P<0.05; **, P<0.01; scale bars are 50 μm)

numbers from each mouse kidney, using kidney cortex and glomeruli (**Figure 2E**, **Supplemental Figure 3A**). The gene encoding PKR, *Eif2ak2*, was expressed in glomeruli and all tubular segments (**Supplemental Figure 3B**).

Downregulation of mitochondrial genes in Tg26 kidneys

GSEA results of bulk RNA-seq showed that mitochondrial-related pathways were the most downregulated pathway in Tg26 mice when compared with WT mice, suggesting that mitochondrial gene transcription (for both nuclear-genome and mitochondrial genome-encoded genes) was significantly downregulated (**Figure 3A**). Expression levels of specific mitochondrial genes were assessed (**Figure 3B**) and showed that C16 treatment reversed the downregulation of these mitochondrial genes (**Figure 3B, 3C**). Western blot analyses were consistent with bulk RNA-seq results showing lower abundance of mitochondrial complex I and II in Tg26 kidney and this was restored to normal by C16 treatment (**Figure 3D**, **Supplemental Figure 4A-D**). Mitochondrial DNA copy numbers were decreased in Tg26 mice, but C16 treatment did not reverse these changes (**Supplemental Figure 4E, 4F**).

These findings suggest that PKR inhibition by C16 rescued transcriptional downregulation of both nuclear-encoded and mitochondrial-encoded mitochondrial genes, but the rescue was not through increased mitochondrial DNA copy number. Single-nucleus RNA-seq and subsequent pathway analysis showed that the majority of cell types, including mitochondrial proximal tubules (PT-Mito), PT-S1, injured PT (PT-Inj), and endothelial cells, manifested global downregulation of mitochondrial-expressed genes in Tg26 kidneys and that this decline was rescued by C16 treatment (**Figure 3E**).

Novel proximal tubular cell cluster with high mitochondrial gene expression

Based on unbiased clustering, we identified a distinct proximal tubule cell cluster characterized by higher expression level of mitochondrial genes (PT-Mito) and consisting of 3.1-5.8% of kidney cortex cells (**Figure 2E**). We analyzed the seven proximal tubular cell clusters and found distinctive markers that distinguish each cluster (**Figure 4A**). Based on UMAP, this PT-Mito cluster was in proximity to proximal tubule-segment1 (PT-S1) and proximal tubule-segment2 (PT-S2) (**Figure 2C**). To confirm the presence of cells giving rise to this cluster, *in situ* hybridization (ISH) of mt-*Co1* and mt-*Atp6* were performed. We observed transcripts inside some nuclei in many putative PT-Mito segments with high expression of these genes (**Figure 4B, 4C**, **Supplemental Figure 5A, 5B**). We also confirmed the existence of similar PT-Mito cluster in published human kidney single-nuclear RNA-seq data[47] by the re-analysis of the original data (**Supplemental Figure 6A-C**).

As the PT-Mito cluster was observed in both WT and Tg26 kidney in similar ratios, this new cluster could be a conserved tubular cell cluster, likely not previously reported due to mitochondrial gene filtering criteria implemented in single-nucleus RNA-seq analytic pipelines. Pathway analysis of snRNA-seq data showed that oxidative phosphorylation genes were downregulated in this PT-Mito cluster in Tg26 mice, compared to wild-type mice, with a Z-score of −4.123. These genes were also downregulated in other many cell types (**Figure 4D**). These findings suggested that mitochondrial dysfunction represents a prominent mechanistic pathway that was dysregulated in majority of cell clusters in Tg26 mice, and that mitochondrial dysfunction was pronounced in the PT-Mito cluster.

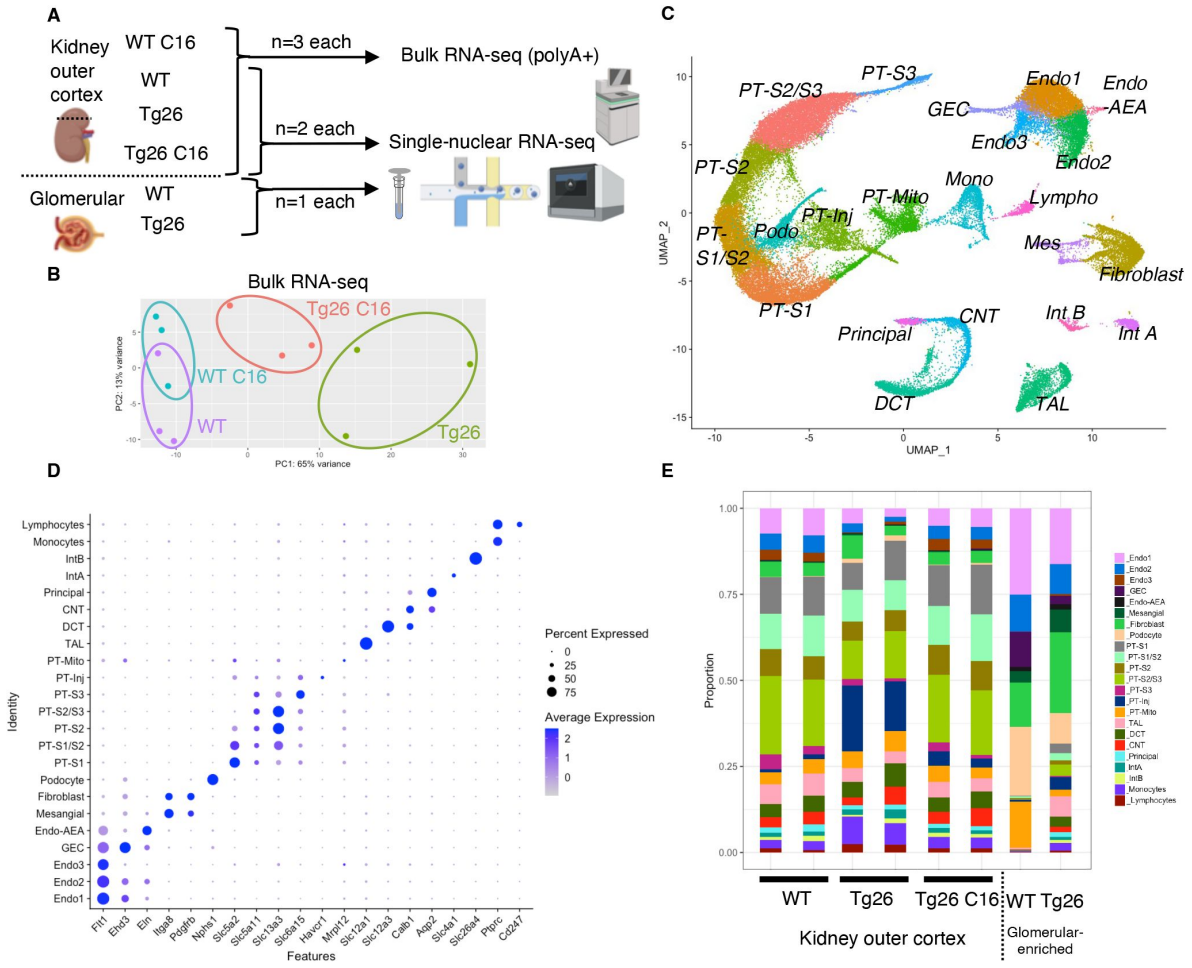

Figure. 2

Overview of bulk RNA-seq and single-nucleus RNA-seq experiments.

(**A**) Shown is the workflow of the bulk RNA-seq and single-nucleus RNA-seq experiments. (**B**) Principal component analysis plot of bulk RNA-seq results. (**C**) UMAP plot of single-nuclear RNA-seq data from 8 samples, 56,976 nuclei, showing 23 clusters. (**D**) Shown is a dot plot of 23 marker genes, each characteristic for the cluster. (**E**) Shown is the ratio of nuclei grouped to each cluster in each sample.

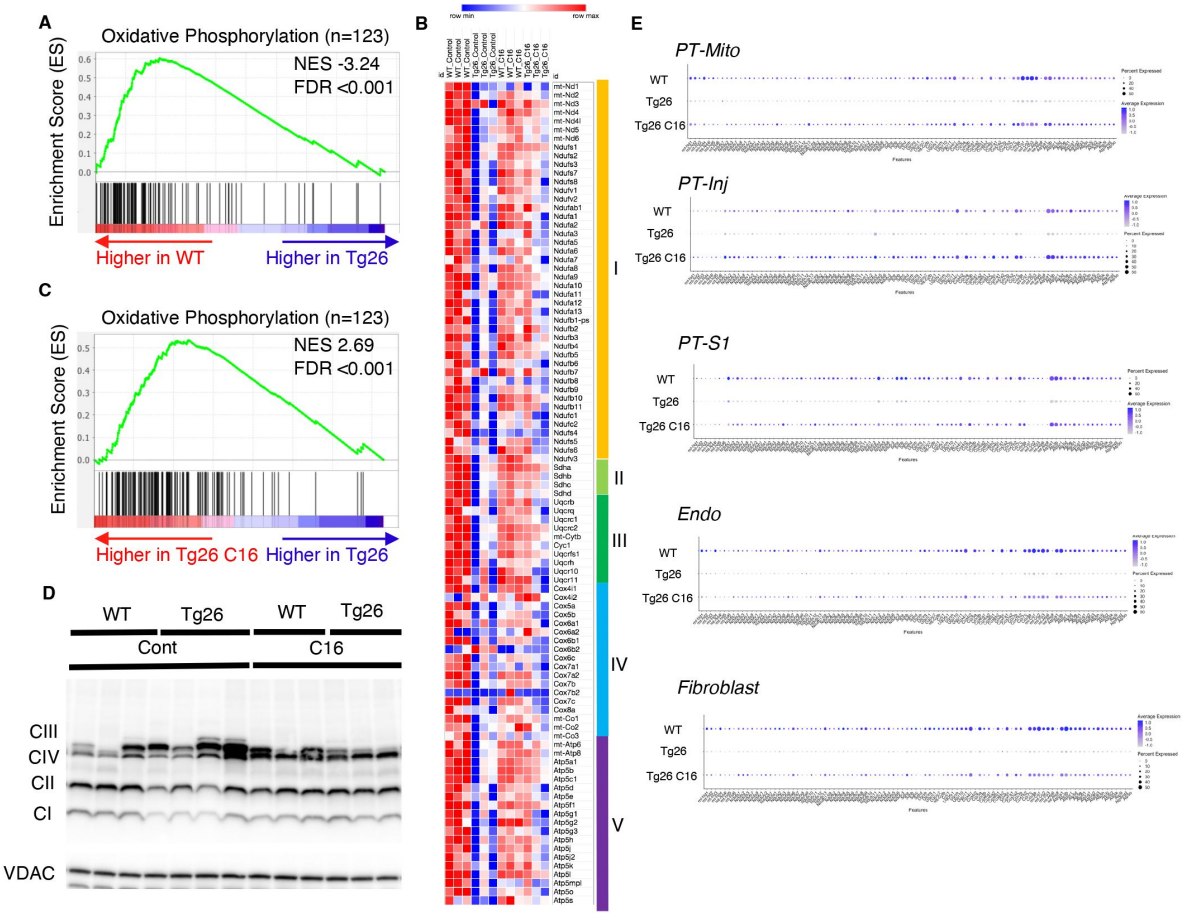

Figure. 3

Oxidative phosphorylation genes are downregulated in Tg26 mice and downregulation is reversed by PKR inhibition using C16.

(**A**) Shown is the enrichment plot of oxidative phosphorylation pathway based on bulk mRNA-seq comparing Tg26 and WT. (**B**) Shown is the enrichment plot of oxidative phosphorylation pathway based on bulk mRNA-seq comparing C16 treated Tg26 and Tg26. (**C**) Heatmap of expressed genes in oxidative phosphorylation pathway (n=123), based on data from bulk mRNA-seq. (**D**) Western blot to identify mitochondrial subunits CI through CIV and VDAC. (**E**) Dot plot showing expression of oxidative phosphorylation pathway genes in PT-Mito, PT-S1, PT-Inj, Endo, and Fibroblast cluster by snRNA-seq.

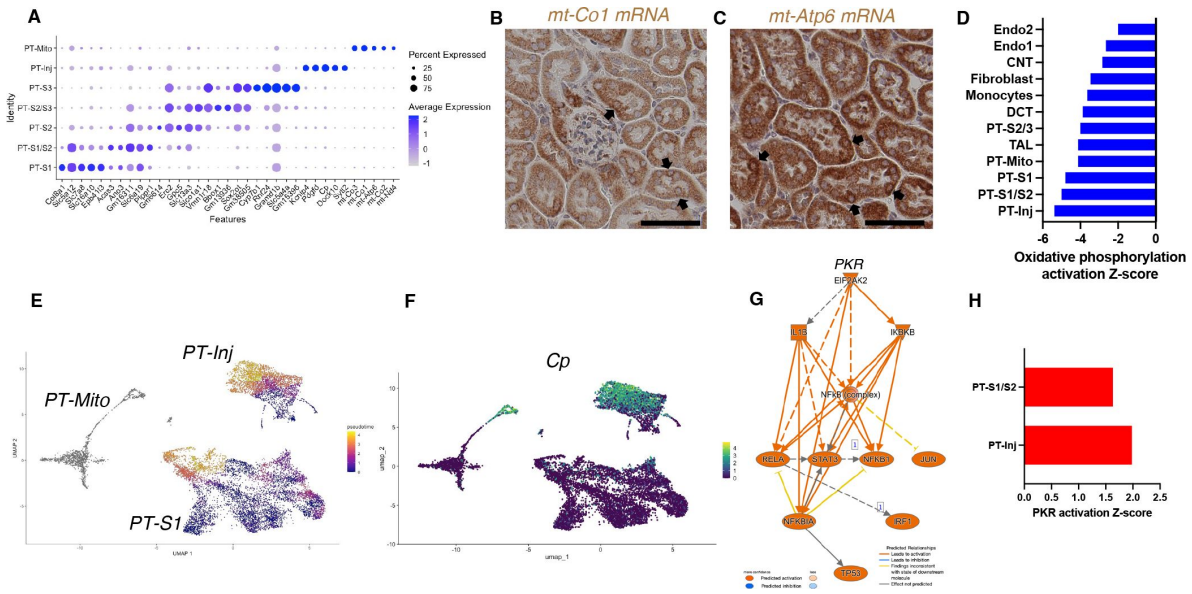

Figure. 4

PT-Mito and PT-Inj cluster characterization.

(**A**) Shown are dot plots showing the top five marker genes in each of the PT clusters (PT-S1, PT-S1/S2, PT-S2, PT-S2/S3, PT-S3, PT-Inj, PT-Mito). (**B, C**) *In situ* hybridization of *mt-Co1* and *mt-Atp6* genes showed signals inside nuclei of WT mice. (Scale bars are 50 μm) (**D**) Shown is the activation Z-score of the oxidative phosphorylation pathway by pathway analysis of each cluster comparing Tg26 vs WT mice. (**E**) Trajectory analysis results including PT-S1, PT-Mito, PT-Inj from WT and Tg26 mice. (**F**) Ceruloplasmin (*Cp*) expression in the trajectory analysis plot. (**G**) PKR downstream pathway mapping by IPA comparing Tg26 vs WT by bulk mRNA-seq data. (**H**) Activation Z-score of PKR pathway by IPA in each cluster comparing Tg26 vs WT.

Proximal tubular cells with injury were more frequent in Tg26 mice

We identified a proximal tubular cell cluster, enriched for injury markers (PT-Inj), which was increased in cell number and percentage in Tg26 mice when compared with WT mice and C16 treated-Tg26 mice. The gene expression profile of this cluster was comparable to profiles previously-reported mouse models of acute kidney injury (AKI)[40] and kidney fibrosis.[48] We compared gene expression in Tg26 mice with previously reported expression of marker genes in injured proximal tubules from snRNA-seq data obtained from a mouse ischemia-reperfusion injury model (**Supplemental Figure 7A**). We found some overlap in these two models (Tg26, ischemia-reperfusion), and the higher expression of these genes in Tg26 mice was ameliorated with C16 treatment (**Supplemental Figure 7B**). This finding suggested some overlap of pathological molecular pathways between HIV-associated tubular injury and ischemic injury, especially at later stages when fibrosis appears.

Pseudotime analysis suggested that injured proximal tubular epithelial cells likely originated from PT-S1 segments, suggesting proximal tubular damage in Tg26 mouse kidneys (**Figure 4E, 4F**). Differential gene expression analysis and IPA upstream analysis of bulk RNA-seq data from Tg26 and wild type mouse kidneys showed activation of the PKR pathway (**Figure 4G**). The per cluster upstream analysis of snRNA-seq data showed the highest PKR pathway activation in PT-Inj (**Figure 4H**).

PKR inhibition rescued Stat3 activation in Tg26 mice

PKR inhibition, acting to reduce inflammatory pathway activation, may influence other important mediators of HIVAN pathophysiology. To identify possible mediators, we used upstream analysis in IPA. We compared C16-treated WT vs WT, Tg26 vs WT, and C16-treated Tg26 vs Tg26, using differential gene expression analysis. All genes with multiple-testing adjusted p-values <0.05 were included in this analysis. An activated Z-score was calculated for each candidate upstream regulator. Candidate transcription factors were sorted in the order of triple Z-score, which was calculated by multiplying the three Z-scores (**Supplemental Figure 8**).

Stat3 and representative examples of Stat3-regulated gene expressions profiles are shown for each tissue comparison (**Figure 5A, 5B**). Interestingly, Stat3 was the most activated upstream regulator and is a well-characterized transcriptional regulator in kidney disease, including in the Tg26 mouse model.[19] We confirmed Stat3 activation through phosphorylation by Western blot showing increased phosphorylation (**Figure 5C, 5D**) and immunohistochemistry (**Figure 5E-G**). These data suggest that PKR inhibition may be therapeutic for Tg26 kidney disease, promoting deactivation of Stat3 and downstream inflammatory pathways. Based on single-nucleus RNA-seq and IPA upstream analysis, we confirmed that Stat3 was activated in the majority of cell types in Tg26 and especially in PT-Inj (**Figure 5H**). As Stat3 translocate to mitochondria and alter cell metabolism[49], Stat3 may also be important mitochondrial regulator in the pathogenesis of HIVAN.

PKR inhibition restored reduced mitochondrial respiration capacity in Tg26

These data shown indicated that mitochondrial-expressed gene transcription was inhibited in the kidney cortex of Tg26 mice and was rescued by PKR inhibition. To investigate mitochondrial functions in kidney, we prepared enriched glomerular and proximal tubular tissue extracts. These were tested for mitochondrial respiratory capacity using the Seahorse extracellular flux analyzer. The results showed reduced maximum respiration and spare respiratory capacity in Tg26 compared to wild-type mice (**Figure 6A-C**). Reduced respiratory capacity in Tg26 mice was rescued by C16 treatment, suggesting that PKR inhibition restored impaired mitochondrial

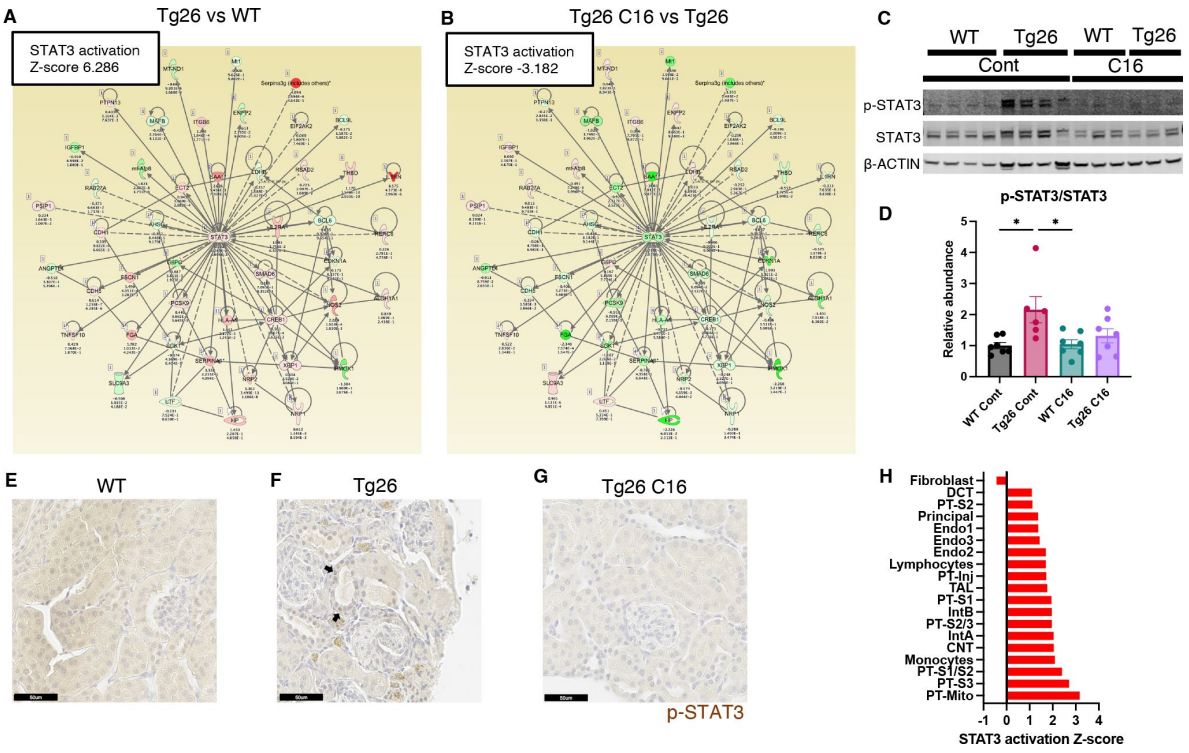

Figure. 5

STAT3 activation downstream of PKR.

(**A, B**) Shown is mapping of STAT3 regulating genes comparing Tg26 vs WT (Z-score 6.286), Tg26 C16 vs Tg26 (Z-score −3.182) by bulk mRNA-seq. Red color indicates upregulation and green color indicates downregulation, quantified as log2-fold change, p-value; and adjusted p-value by false discovery rate are shown. Solid line indicates known positive regulation, dotted line indicates known negative regulation. (**C**) Representative immunoblotting of phospho-STAT3, STAT3 and β-ACTIN. (**D**) Quantitative results of phospho-STAT3/STAT3 by immunoblotting. (one-way ANOVA; *, P<0.05) (**E-G**) Phospho-STAT3 immunostaining of mouse kidneys is shown (Scale bars are 50 μm). Arrows indicate p-Stat3 detection in injured tubular cells. (**H**) STAT3 activation Z-score by upstream regulator analysis comparing Tg26 vs WT in each cluster by snRNA-seq.

respiration in Tg26 mice. Similarly, proximal tubular tissue *ex vivo* also showed lower maximum respiration and less spare respiratory capacity in Tg26 mice compared to wild-type mice (**Figure 6D-F**); both parameters were normalized by C16 treatment. Thus, PKR inhibition rescues mitochondrial dysfunction in both glomerular and proximal tubular cells.

Podocytes in Tg26 mice showed high HIV-1 gene expression with podocyte loss

Although the Tg26 mouse is a well-characterized model of HIVAN, expression levels of each of the HIV-1 genes in single kidney cells has not been previously reported. Using single-nucleus RNA-seq, we annotated expression of each HIV-1 gene, with the aim to quantify HIV-1 gene expression at single cell resolution (**Figure 7A**). Among all kidney cell types, HIV-1 genes were expressed at high levels in podocytes, consistent with the notion that HIV-1 gene expression is particularly injurious to podocytes. HIV-1 gene expression data from this study are consistent with the current understanding that *vpr* and *nef* are main contributors to the pathogenesis of HIVAN. Absolute podocyte loss in Tg26 mice, and podocyte recovery with C16 treatment, were also confirmed by p57 staining and podocyte estimation using the podometric analysis implemented in PodoCount (**Figure 7B-E**).

Podocytes in Tg26 mice showed dedifferentiation and dysregulation of cytoskeleton-related pathways

Since podocytes in Tg26 mice expressed the HIV-1 genes *vpr* and *nef*, we investigated related pathways that were dysregulated in podocytes. The yield of podocytes from kidney cortex samples was relatively low and, therefore, we used snRNA-seq data from isolated glomeruli from wild-type and Tg26 mice, which enriched podocytes. Pseudotime analysis of these data showed progression in transcripts from wild-type podocytes to the majority of Tg26 podocytes, showing *nef* expression in most injured Tg26 podocytes (**Figure 7F, 7G**). Differential expression analysis and pathway analysis suggested that in Tg26 mice, Rho protein dissociation inhibitors (RHOGDI) signaling and corona virus pathogenesis pathways were activated, while integrin and actin cytoskeleton signaling pathways were deactivated (**Figure 7H**).

These findings are consistent with previous reports and with a common conceptual model in which podocyte dedifferentiation starts with cytoskeletal changes and progresses to cell detachment from the glomerular tuft.[50–52] We confirmed dedifferentiation of podocytes in Tg26 mice by showing down-regulation of podocyte markers and reversal or prevention of dedifferentiation in Tg26 mice treated with C16 (**Figure 7I**). This was also demonstrated histologically by p57 staining, which was lost in Tg26 and then regained following C16 treatment (**Figure 7B-D**). We also found increased expression of *Ccn2* (encoding cellular communication network factor 2), an epithelial–mesenchymal transition (EMT) marker, in Tg26 podocytes. This is consistent with the signatures that we previously reported in urine podocytes in a single-cell clinical study of FSGS patients.[53] We also observed upregulation of *Rbfox1*, encoding RNA-binding fox-1 homolog-1, as candidate disease marker in Tg26 podocytes (**Figure 7I**). Rbfox1 also regulates key neuronal functions.[54,55]

Expression of integrin subunits *Itga4* and of *Spp1* (encoding osteopontin) and *Tgfb2* (encoding transforming growth factor β2) was also upregulated in Tg26 podocytes, indicating activation of cell adhesion and pro-fibrotic processes (**Figure 7I**). We compared gene expression in *nef*-positive podocytes (24 cells) and *nef-negative* podocytes (480 cells) from Tg26 glomerular data, to confirm the association between HIV-1 gene expression and transcriptomic changes. We found lower expression of canonical podocyte marker genes, including *Nphs1*, *Synpo*, together with higher expression of *Rbfox1* and *Spp1* described above (**Figure 7J**).

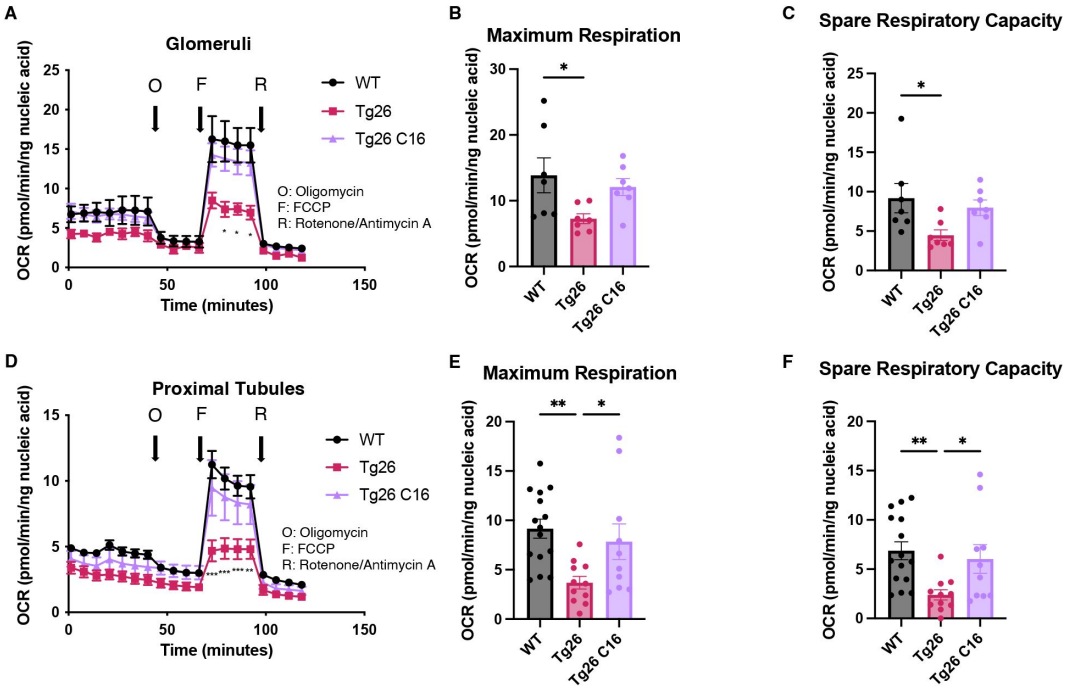

Figure. 6

PKR inhibition with C16 reverses mitochondrial dysfunction in Tg26 glomeruli and proximal tubules.

(**A**) Shown are oxygen consumption rate (OCR) measurements during cell mitochondrial stress testing, using extracted glomeruli from WT, Tg26, and C16 Tg26 kidney tissue. (**B**) Maximum respiration rate was calculated by OCR measurements of glomeruli. (**C**) Spare respiratory capacity was calculated by OCR measurements of glomeruli. (**D**) Shown are oxygen consumption rate (OCR) measurements during cell mitochondrial stress testing, using extracted proximal tubules from WT, Tg26, and C16 Tg26 kidney tissue. (**E**) Maximum respiration rate was calculated by OCR measurements of isolated proximal tubules. (**F**) Spare respiratory capacity was calculated by OCR measurements of isolated proximal tubules. (One-way ANOVA; *, P<0.05; **, P<0.01)

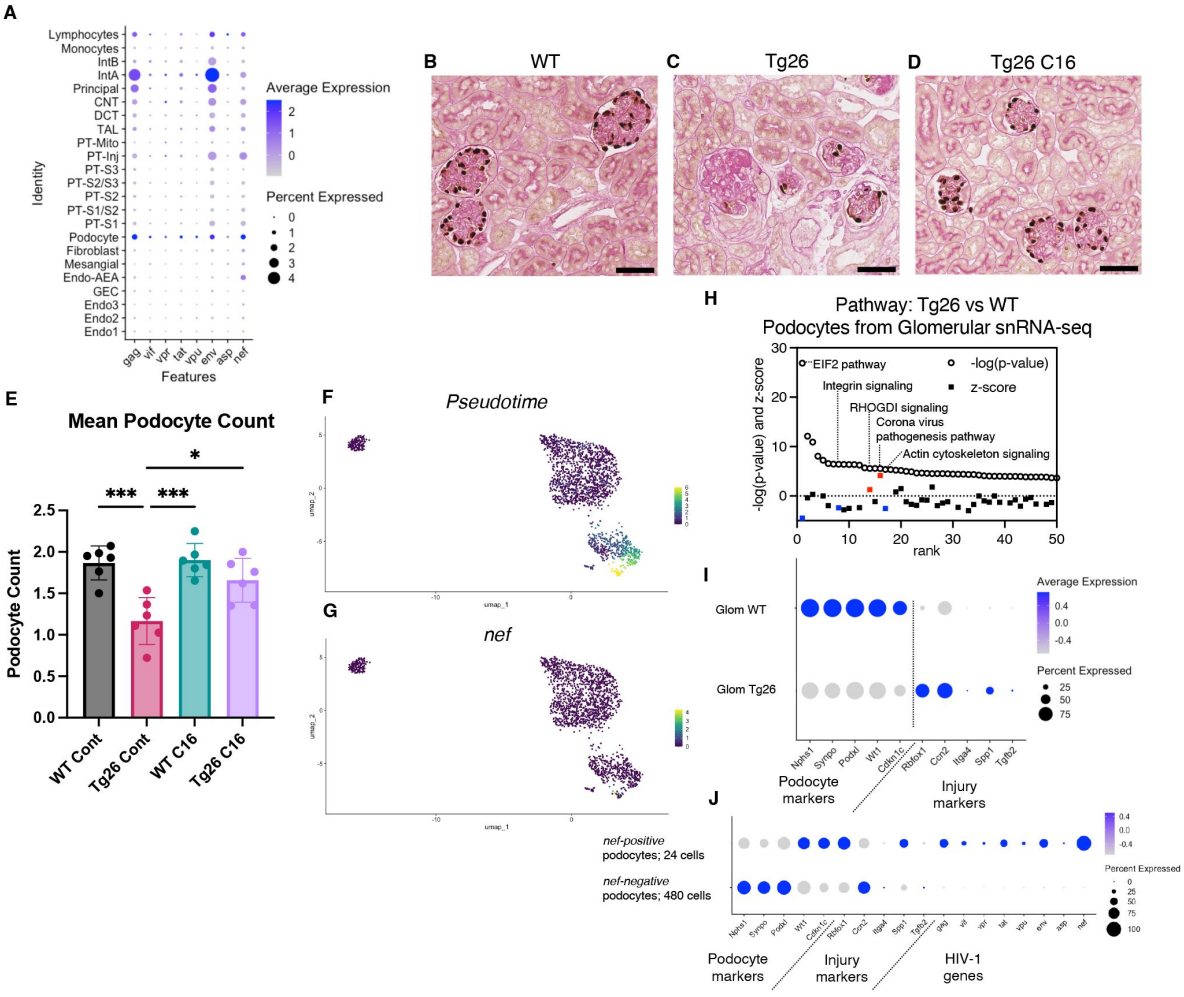

Figure. 7

HIV-1 gene expression causes Tg26 podocytes dedifferentiation.

(**A**) Shown is dot plot demonstrating HIV-1 gene expression levels in each cluster detected by snRNA-seq. (**B-D**) p57 staining of kidney showing podocyte loss and dedifferentiation. (Scale bars are 50 μm) (**E**) Podocount analysis showed podocyte loss in Tg26 and was rescued by C16. (One-way ANOVA; *, P<0.05; ***, P<0.001) (**F**) Trajectory analysis of podocytes by snRNA-seq data from WT, Tg26 glom samples. (**G**) Trajectory map showing *nef* expression. (**H**) Pathway analysis results by IPA comparing Tg26 vs WT using glomerular snRNA-seq data from podocyte cluster. (**I**) Dot plot showing podocyte marker genes and representative differentially expressed genes in podocytes by glomerular snRNA-seq. (**J**) Dot plot comparing expression of representative genes in glomerular Tg26 podocytes between *nef*-positive and *nef*-negative podocytes.

Tg26 kidney cells showed active cell-cell interaction

To investigate pathologic cell-cell interactions in Tg26 kidneys and the ameliorative effect of PKR inhibition, we performed cell-cell interaction analysis using the snRNA-seq data. The expression heatmap suggested changes in cell-cell interaction in each sample at the resolution of each identified cell cluster (**Supplemental Figure 9A-C**). We sought candidate cell types that might contribute to Tg26 pathology and found candidate ligand-receptor pairs (**Figure 8A-C**). For example, platelet derived growth factor D (PDGF-D) was upregulated in PT-Inj in Tg26 mice and was downregulated by C16 treatment (**Figure 8D**). Further, PDGF-D may interact with PDGFR-B in fibroblasts. Immunohistochemistry demonstrated the presence of PDGF-D in the vicinity of dilated tubules (**Figure 8E, 8F**). As PDGF-D is known to be induced by STAT3, these findings identified a potential fibrogenic pathway triggered by PKR activation in PT-Inj.

Discussion

This work, applying combined analysis of single-nucleus RNA-seq and bulk RNA-seq data, highlight the role of PKR activation in the Tg26 HIVAN mouse model and show mitochondrial dysfunction to be one of the most dysregulated pathways. Mitochondrial dysfunction in Tg26 mouse glomeruli and myocytes has been previously reported.[24,56] The present study demonstrated by single-nucleus RNA-seq and Seahorse bioenergetics assay that mitochondrial dysfunction is induced in various cell types in Tg26 kidney, especially proximal tubular cells and endothelial cells. It is likely that HIVAN tubular pathology is mediated, at least in part, by mitochondrial dysfunction in proximal tubular cells, and that glomerular mitochondrial dysfunction is mainly confined to endothelial cells. Further, PKR activation may be one of several processes that contributes to mitochondrial dysfunction in HIVAN. A recent report using tubular cell-specific Vpr overexpression mouse model has shown that mitochondrial dysfunction is implicated in tubular injury. Our findings are congruent with this report.[57]

Further, single-nucleus RNA-sequencing of Tg26 kidney cortex identified a novel mitochondrial gene-enriched proximal tubular cell population (PT-Mito). This cell population had not been previously recognized, likely due to filtering criteria routinely employed to reduced mitochondrial genome-encoded transcript levels in single-cell/single nucleus datasets. It has been well established that a high percentage of mitochondrial transcripts captured in single-cell RNA-seq studies suggests stressed cells, and these cells are typically excluded from analysis. However, in single-nucleus RNA-seq data sets, mitochondrial gene percentage is generally low following the nuclear purification. Most nuclei captured have mitochondrial transcripts levels of <1% of the total transcripts captured. Therefore, we did not filter out mitochondrial transcripts entirely from the analysis but excluded nuclei with >20% mitochondrial transcripts.[58] By not filtering out mitochondrial genes in the analysis, we found dysregulation of these transcripts, providing clues to pathogenesis.

We further demonstrated by ISH the presence of mitochondrial transcripts in nuclei whose cells were identified in single-nuclei analysis of the same tissue samples. Although we cannot completely exclude the possibility of having captured some mitochondria during nuclear preparation, we confirmed expression of nuclear genes, such as *Gpx1* and *Gpx3*, which were also highly expressed in this PT-Mito cluster. A relatively high abundance of mitochondrial transcripts in the PT-Mito cluster may indicate the existence of mitochondrial transcripts that were transported into nuclei. This PT-Mito cluster might have remained previously undetected because of the similarity of its transcripts with that of those other proximal tubules and the lack of cell type-specific markers. Considering the high mitochondrial gene expression levels and corresponding mitochondrial pathway dysregulation in Tg26 mice, this PT-Mito cluster may represent the most metabolically active cells, which are also the most highly vulnerable cell type

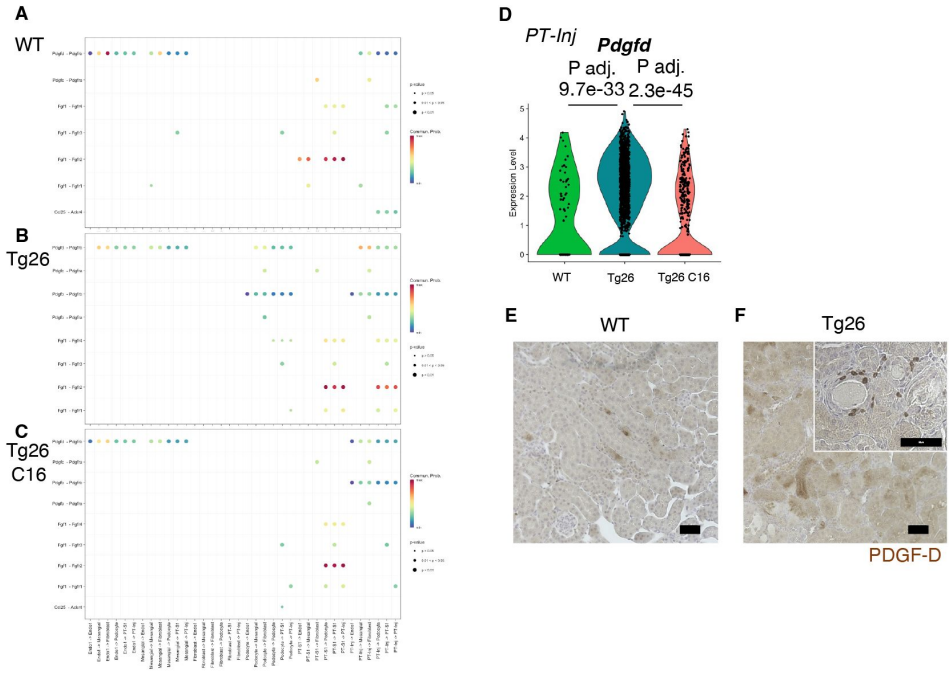

Figure. 8

Cell-cell interaction analysis shows activated ligand-receptor interaction: PDGF-D-PDGFR-B pathway in Tg26.

(**A-C**) Shown are dot plots depicting results from cell-cell interaction analysis of WT, Tg26, C16 Tg26 snRNA-seq data. (**D**) Violin plots showing *Pdgfd* expression levels in the PT-Inj cluster. (**E, F**) PDGF-D immunostaining of mouse kidneys is shown. (Scale bars are 50 μm)

in proximal tubules. Nevertheless, considering the downregulation of both nuclear and mitochondrial encoded genes involved in oxidative phosphorylation; mitochondrial dysfunction likely plays a major role in the pathology of HIVAN.

Another novel finding arose from investigating HIV-1 gene expression in the Tg26 mouse. Transcripts for all transgene-encoded HIV-1 genes were detected in all cell types examined, albeit some transcripts were present at low expression levels. This included transcripts for *nef* and *vpr* that are, according to current understanding, the main contributors to HIVAN.[59,60] Podocytes showed the highest levels of transgene expression, which is consistent with the prominent pathology observed in podocytes. This finding suggests a shared but unknown mechanism in virus-related nephropathies with podocyte damage. One possible explanation for podocytes not showing overt mitochondrial gene dysregulation despite high HIV-1 gene expression (compared to proximal tubular cells and endothelial cells) is a possible tighter regulation of mitochondrial gene expression in podocytes, as suggested by Li et al.[61] With regard to S phase-specific genes[62], we did not find a consistent expression change in cells including podocytes from the glomerular sample (**Supplemental Figure 3G**).

Further, we identified a putative activated pathway involving PKR - STAT3 - PDGF-D - PDGFR-B in injured proximal tubules. The PKR-STAT3-PDGF signaling cascade has been reported in PKR-null mouse embryonic fibroblasts.[63] PDGF-D and PDGFR-B contribute to fibrosis in glomeruli and the tubulointerstitium in experimental animal studies [64,65]. Inhibiting this pathway may offer an avenue to reduce kidney injury in HIVAN. Further studies will be needed to confirm whether this mechanism is shared with human HIVAN or other RNA virus-associated kidney diseases.

The present study has limitations. First, the Tg26 mouse model involves a partial HIV-1 transgene that may not recapitulate all aspects of clinical HIVAN. Second, gene expression changes after C16 treatment may include changes secondary to the attenuated renal injury, in addition to the direct effect of C16. Third, we acknowledge possibility of a non-specific effect of C16 as an inhibitor of PKR.[66–68]

In conclusion, by combining single-nucleus RNA-seq and bulk RNA-seq analysis, we identified mitochondrial dysfunction as the central mechanism for proximal tubule injury in the Tg26 HIVAN mouse model. This process that was largely reversed by treatment with the PKR inhibitor C16. Further studies of HIVAN-associated mitochondrial dysfunction may lead to targeted therapeutics.

Author Contributions

TY, KO, JBK conceived the study design. TY conducted mouse experiments with support by SS. TY analyzed bulk RNA-seq data. TY and YY conducted single-nuclear RNA-seq capture. TY and KZL analyzed single-nuclear RNA-seq data. YZ and CAW supported sequencing at FNLCR/NCI. AZR assessed pathological quantification. BS, TY, VT and PS conducted podocyte morphometry. KM, BJ, XW conducted OXPHOS complex Western blot. TY, JBK drafted the manuscript and all the authors contributed for edits. The order of the co-first authors was based on when they started on the project and the relative contribution to the authoring of the original version of the manuscript.

Acknowledgements

We thank the Sequencing Facility and Bioinformatics Group (Frederick National Laboratory for Cancer Research (FNLCR), NCI, NIH) for sequencing and informatics support, Drs. Joon-Yong Chung and Stephen M. Hewitt (NCI/NIH) for whole slide scanning, Maria Campos (NEI/NIH) for pathological service, Dr. Daria Ilatovskaya (Medical University of South Carolina) for suggestion of

Seahorse assay, and Drs. Mark A. Knepper (NHLBI, NIH), Gregory G. Germino (NIDDK, NIH) and Michael J. Ross (Albert Einstein College of Medicine) for scientific suggestions and supports, Dr. Jurgen Heymann for critical manuscript review. This work utilized the computational resources of the NIH HPC Biowulf cluster. (*http://hpc.nih.gov*) Part of this work was presented at American Society of Nephrology Kidney Week 2020, 2021. The content of this publication does not necessarily reflect the views or policies of the Department of Health and Human Services, nor does mention of trade names, commercial products, or organizations imply endorsement by the U.S. Government.

Funding

This project has been funded in part with federal funds from the National Cancer Institute, National Institutes of Health, under contract 75N91019D00024. The work was also supported by the Intramural Research Program of the NIH, including the National Cancer Institute, Center for Cancer Research and the NIDDK.

Data Availability

Original data files and count tables have been deposited in GEO (GSE205060). Other data are available from the authors upon request.

References

1. Fauci AS. (2021) **NIH Statement on World AIDS Day**

2. Centers for Disease Control and Prevention (2019) **HIV Surveillance Report**

3. Dwyer-Lindgren L, Cork MA, Sligar A, et al. (2019) **Mapping HIV prevalence in sub-Saharan Africa between 2000 and 2017** *Nature* **570**:189–193 https://doi.org/10.1038/s41586-019-1200-9

4. Palau L, Menez S, Rodriguez-Sanchez J, et al. (2018) **HIV-associated nephropathy: links, risks and management** *HIV AIDS (Auckl* **10**:73–81 https://doi.org/10.2147/HIV.S141978

5. Menez S, Hanouneh M, McMahon BA, Fine DM, Atta MG (2018) **Pharmacotherapy and treatment options for HIV-associated nephropathy** *Expert Opin Pharmacother* **19**:39–48 https://doi.org/10.1080/14656566.2017.1416099

6. Yahaya I, Uthman OA, Uthman MM (2013) **Interventions for HIV-associated nephropathy** *Cochrane Database of Systematic Reviews* https://doi.org/10.1002/14651858.CD007183.pub3

7. Bruggeman LA, Dikman S, Meng C, Quaggin SE, Coffman TM, Klotman PE (1997) **Nephropathy in human immunodeficiency virus-1 transgenic mice is due to renal transgene expression** *J Clin Invest. Jul* **100**:84–92 https://doi.org/10.1172/JCI119525

8. Dickie P, Felser J, Eckhaus M, et al. (1991) **HIV-associated nephropathy in transgenic mice expressing HIV-1 genes** *Virology* **185**:109–19 https://doi.org/10.1016/0042-6822(91)90759-5

9. Kopp JB, Klotman ME, Adler SH, et al. (1992) **Progressive glomerulosclerosis and enhanced renal accumulation of basement membrane components in mice transgenic for human immunodeficiency virus type 1 genes** *Proc Natl Acad Sci USA.* **89**:1577–81 https://doi.org/10.1073/pnas.89.5.1577

10. Kumar D, Konkimalla S, Yadav A, et al. (2010) **HIV-associated nephropathy: role of mammalian target of rapamycin pathway** *Am J Pathol* **177**:813–21 https://doi.org/10.2353/ajpath.2010.100131

11. Yadav A, Kumar D, Salhan D, et al. (2012) **Sirolimus modulates HIVAN phenotype through inhibition of epithelial mesenchymal transition** *Exp Mol Pathol* **93**:173–81 https://doi.org/10.1016/j.yexmp.2012.04.021

12. Rai P, Plagov A, Lan X, et al. (2013) **mTOR plays a critical role in p53-induced oxidative kidney cell injury in HIVAN** *Am J Physiol Renal Physiol* **305**:F343–F354 https://doi.org/10.1152/ajprenal.00135.2013

13. Sharma M, Magenheimer LK, Home T, et al. (2013) **Inhibition of Notch pathway attenuates the progression of human immunodeficiency virus-associated nephropathy** *Am J Physiol Renal Physiol* **304**:F1127–F1136 https://doi.org/10.1152/ajprenal.00475.2012

14. Puri RV, Yerrathota S, Home T, et al. (2019) **Notch4 activation aggravates NF-kappaB-mediated inflammation in HIV-1-associated nephropathy** *Dis Model Mech* **12** https://doi.org/10.1242/dmm.040642

15. Zhong Y, Chen EY, Liu R, et al. (2013) **Renoprotective effect of combined inhibition of angiotensin-converting enzyme and histone deacetylase** *J Am Soc Nephrol* **24**:801–11 https://doi.org/10.1681/ASN.2012060590

16. Rai P, Lederman R, Haque S, et al. (2014) **Renin angiotensin system modulates mTOR pathway through AT2R in HIVAN** *Exp Mol Pathol* **96**:431–7 https://doi.org/10.1016/j.yexmp.2014.04.004

17. Gherardi D, D'Agati V, Chu TH, et al. (2004) **Reversal of collapsing glomerulopathy in mice with the cyclin-dependent kinase inhibitor CYC202** *J Am Soc Nephrol* **15**:1212–22 https://doi.org/10.1097/01.asn.0000124672.41036.f4

18. Wang X, Liu R, Zhang W, et al. (2020) **Role of SIRT1 in HIV-associated kidney disease** *Am J Physiol Renal Physiol* **319**:F335–F344 https://doi.org/10.1152/ajprenal.00140.2020

19. Feng X, Lu TC, Chuang PY, et al. (2009) **Reduction of Stat3 activity attenuates HIV-induced kidney injury** *J Am Soc Nephrol* **20**:2138–46 https://doi.org/10.1681/asn.2008080879

20. Gu L, Dai Y, Xu J, et al. (2013) **Deletion of podocyte STAT3 mitigates the entire spectrum of HIV-1-associated nephropathy** *AIDS* **27**:1091–1098 https://doi.org/10.1097/QAD.0b013e32835f1ea1

21. Ratnam KK, Feng X, Chuang PY, et al. (2011) **Role of the retinoic acid receptor-α in HIV-associated nephropathy** *Kidney Int* **79**:624–634 https://doi.org/10.1038/ki.2010.470

22. Zhang G, Liu R, Zhong Y, et al. (2012) **Down-regulation of NF-kappaB transcriptional activity in HIV-associated kidney disease by BRD4 inhibition** *J Biol Chem* **287**:28840–28851 https://doi.org/10.1074/jbc.M112.359505

23. Haque S, Lan X, Wen H, et al. (2016) **HIV Promotes NLRP3 Inflammasome Complex Activation in Murine HIV-Associated Nephropathy** *Am J Pathol* **186**:347–58 https://doi.org/10.1016/j.ajpath.2015.10.002

24. Bryant JL, Guda PR, Asemu G, et al. (2018) **Glomerular mitochondrial changes in HIV associated renal injury** *Exp Mol Pathol* **104**:175–189 https://doi.org/10.1016/j.yexmp.2018.03.004

25. Katuri A, Bryant JL, Patel D, et al. (2019) **HIVAN associated tubular pathology with reference to ER stress, mitochondrial changes, and autophagy** *Exp Mol Pathol* **106**:139–148 https://doi.org/10.1016/j.yexmp.2018.12.009

26. Jin Y, Ratnam K, Chuang PY, et al. (2012) **A systems approach identifies HIPK2 as a key regulator of kidney fibrosis** *Nat Med.* **18**:580–588 https://doi.org/10.1038/nm.2685

27. Liu R, Das B, Xiao W, et al. (2017) **A Novel Inhibitor of Homeodomain Interacting Protein Kinase 2 Mitigates Kidney Fibrosis through Inhibition of the TGF-beta1/Smad3 Pathway** *J Am Soc Nephrol* **28**:2133–2143 https://doi.org/10.1681/ASN.2016080841

28. Xiao W, Jing E, Bao L, et al. (2020) **Tubular HIPK2 is a key contributor to renal fibrosis** *JCI Insight.* **5** https://doi.org/10.1172/jci.insight.136004

29. Fan Y, Wei C, Xiao W, et al. (2014) **Temporal profile of the renal transcriptome of HIV-1 transgenic mice during disease progression** *PLoS One* **9** https://doi.org/10.1371/journal.pone.0093019

30. Okamoto K, Rausch JW, Wakashin H, et al. (2018) **APOL1 risk allele RNA contributes to renal toxicity by activating protein kinase R** *Commun Biol* **1** https://doi.org/10.1038/s42003-018-0188-2

31. Tronel C, Page G, Bodard S, Chalon S, Antier D (2014) **The specific PKR inhibitor C16 prevents apoptosis and IL-1beta production in an acute excitotoxic rat model with a neuroinflammatory component** *Neurochem Int* **64**:73–83 https://doi.org/10.1016/j.neuint.2013.10.012

32. Ingrand S, Barrier L, Lafay-Chebassier C, Fauconneau B, Page G, Hugon J (2007) **The oxindole/imidazole derivative C16 reduces in vivo brain PKR activation** *FEBS Lett.* **581**:4473–4478 https://doi.org/10.1016/j.febslet.2007.08.022

33. Kasembeli AN, Duarte R, Ramsay M, et al. (2015) **APOL1 Risk Variants Are Strongly Associated with HIV-Associated Nephropathy in Black South Africans** *J Am Soc Nephrol* **26**:2882–90 https://doi.org/10.1681/asn.2014050469

34. Santo BA, Govind D, Daneshpajouhnejad P, et al. (2022) **PodoCount: A Robust, Fully Automated, Whole-Slide Podocyte Quantification Tool** *Kidney International Reports* **7**:1377–1392 https://doi.org/10.1016/j.ekir.2022.03.004

35. Martin M. (2011) **Cutadapt removes adapter sequences from high-throughput sequencing reads. next generation sequencing; small RNA; microRNA** *adapter removal* **17** https://doi.org/10.14806/ej.17.1.200

36. Love MI, Huber W, Anders S (2014) **Moderated estimation of fold change and dispersion for RNA-seq data with DESeq2** *Genome Biology* **15** https://doi.org/10.1186/s13059-014-0550-8

37. Subramanian A, Tamayo P, Mootha VK, et al. (2005) **Gene set enrichment analysis: a knowledge-based approach for interpreting genome-wide expression profiles** *Proc Natl Acad Sci U S A.* **102**:15545–15550 https://doi.org/10.1073/pnas.0506580102

38. Mootha VK, Lindgren CM, Eriksson KF, et al. (2003) **PGC-1alpha-responsive genes involved in oxidative phosphorylation are coordinately downregulated in human diabetes** *Nat Genet* **34**:267–73 https://doi.org/10.1038/ng1180

39. Kramer A, Green J, Pollard J, Tugendreich S (2014) **Causal analysis approaches in Ingenuity Pathway Analysis** *Bioinformatics.* **30**:523–530 https://doi.org/10.1093/bioinformatics/btt703

40. Kirita Y, Wu H, Uchimura K, Wilson PC, Humphreys BD (2020) **Cell profiling of mouse acute kidney injury reveals conserved cellular responses to injury** *Proc Natl Acad Sci U S A. Jul* **117**:15874–15883 https://doi.org/10.1073/pnas.2005477117

41. Young MD, Behjati S (2020) **SoupX removes ambient RNA contamination from droplet-based single-cell RNA sequencing data** *GigaScience* **9** https://doi.org/10.1093/gigascience/giaa151

42. McGinnis CS, Murrow LM, Gartner ZJ (2019) **DoubletFinder: Doublet Detection in Single-Cell RNA Sequencing Data Using Artificial Nearest Neighbors** *Cell Syst.* **8**:329–337 https://doi.org/10.1016/j.cels.2019.03.003

43. Hao Y, Hao S, Andersen-Nissen E, et al. (2021) **Integrated analysis of multimodal single-cell data** *Cell.* **184**:3573–3587 https://doi.org/10.1016/j.cell.2021.04.048

44. Trapnell C, Cacchiarelli D, Grimsby J, et al. (2014) **The dynamics and regulators of cell fate decisions are revealed by pseudotemporal ordering of single cells** *Nat Biotechnol* **32**:381–386 https://doi.org/10.1038/nbt.2859

45. Jin S, Guerrero-Juarez CF, Zhang L, et al. (2021) **Inference and analysis of cell-cell communication using CellChat** *Nature Communications* **12** https://doi.org/10.1038/s41467-021-21246-9

46. Carpick BW, Graziano V, Schneider D, Maitra RK, Lee X, Williams BR (1997) **Characterization of the solution complex between the interferon-induced, double-stranded RNA-activated protein kinase and HIV-I trans-activating region RNA** *J Biol Chem.* **272**:9510–9516 https://doi.org/10.1074/jbc.272.14.9510

47. Wilson PC, Wu H, Kirita Y, et al. (2019) **The single-cell transcriptomic landscape of early human diabetic nephropathy** *Proc Natl Acad Sci U S A.* **116**:19619–19625 https://doi.org/10.1073/pnas.1908706116

48. Lu YA, Liao CT, Raybould R, et al. (2021) **Single-Nucleus RNA Sequencing Identifies New Classes of Proximal Tubular Epithelial Cells in Kidney Fibrosis** *J Am Soc Nephrol* **32**:2501–2516 https://doi.org/10.1681/asn.2020081143

49. Xu YS, Liang JJ, Wang Y, et al. (2016) **STAT3 Undergoes Acetylation-dependent Mitochondrial Translocation to Regulate Pyruvate Metabolism** *Sci Rep. Dec* **6** https://doi.org/10.1038/srep39517

50. Lu TC, He JC, Wang ZH, et al. (2008) **HIV-1 Nef disrupts the podocyte actin cytoskeleton by interacting with diaphanous interacting protein** *J Biol Chem.* **283**:8173–8182 https://doi.org/10.1074/jbc.M708920200

51. Husain M, D'Agati VD, He JC, Klotman ME, Klotman PE (2005) **HIV-1 Nef induces dedifferentiation of podocytes in vivo: a characteristic feature of HIVAN** *Aids.* **19**:1975–1980 https://doi.org/10.1097/01.aids.0000191918.42110.27

52. Sunamoto M, Husain M, He JC, Schwartz EJ, Klotman PE (2003) **Critical role for Nef in HIV-1-induced podocyte dedifferentiation** *Kidney Int* **64**:1695–701 https://doi.org/10.1046/j.1523-1755.2003.00283.x

53. Latt KZ, Heymann J, Jessee JH, et al. (2022) **Urine Single-Cell RNA Sequencing in Focal Segmental Glomerulosclerosis Reveals Inflammatory Signatures** *Kidney Int Rep* **7**:289–304 https://doi.org/10.1016/j.ekir.2021.11.005

54. Carreira-Rosario A, Bhargava V, Hillebrand J, Kollipara RK, Ramaswami M, Buszczak M (2016) **Repression of Pumilio Protein Expression by Rbfox1 Promotes Germ Cell Differentiation** *Dev Cell.* **36**:562–571 https://doi.org/10.1016/j.devcel.2016.02.010

55. Lee JA, Damianov A, Lin CH, et al. (2016) **Cytoplasmic Rbfox1 Regulates the Expression of Synaptic and Autism-Related Genes** *Neuron.* **89**:113–128 https://doi.org/10.1016/j.neuron.2015.11.025

56. Cheung JY, Gordon J, Wang J, et al. (2019) **Mitochondrial dysfunction in human immunodeficiency virus-1 transgenic mouse cardiac myocytes** *J Cell Physiol* **234**:4432–4444 https://doi.org/10.1002/jcp.27232

57. Chen Y, Chen Y, Fu J, et al. (2023) **Tubular-specific expression of HIV protein Vpr leads to severe tubulointerstitial damage accompanied by progressive fibrosis and cystic development** *Kidney Int* **103**:529–543 https://doi.org/10.1016/j.kint.2022.12.012

58. Slyper M, Porter CBM, Ashenberg O, et al. (2020) **A single-cell and single-nucleus RNA-Seq toolbox for fresh and frozen human tumors** *Nat Med* **26**:792–802 https://doi.org/10.1038/s41591-020-0844-1

59. Zuo Y, Matsusaka T, Zhong J, et al. (2006) **HIV-1 genes vpr and nef synergistically damage podocytes, leading to glomerulosclerosis** *J Am Soc Nephrol* **17**:2832–43 https://doi.org/10.1681/ASN.2005080878

60. Rednor SJ, Ross MJ (2018) **Molecular Mechanisms of Injury in HIV-Associated Nephropathy** *Front Med (Lausanne* **5** https://doi.org/10.3389/fmed.2018.00177

61. Li SY, Park J, Qiu C, et al. (2017) **Increasing the level of peroxisome proliferator-activated receptor γ coactivator-1α in podocytes results in collapsing glomerulopathy** *JCI Insight.* **2** https://doi.org/10.1172/jci.insight.92930

62. Tirosh I, Izar B, Prakadan SM, et al. (2016) **Dissecting the multicellular ecosystem of metastatic melanoma by single-cell RNA-seq** *Science.* **352**:189–96 https://doi.org/10.1126/science.aad0501

63. Deb A, Zamanian-Daryoush M, Xu Z, Kadereit S, Williams BRG (2001) **Protein kinase PKR is required for platelet-derived growth factor signaling of c-fos gene expression via Erks and Stat3** *The EMBO Journal* **20**:2487–2496 https://doi.org/10.1093/emboj/20.10.2487

64. Kok HM, Falke LL, Goldschmeding R, Nguyen TQ. (2014) **Targeting CTGF, EGF and PDGF pathways to prevent progression of kidney disease** *Nat Rev Nephrol* **10**:700–11 https://doi.org/10.1038/nrneph.2014.184

65. Buhl EM, Djudjaj S, Klinkhammer BM, et al. (2020) **Dysregulated mesenchymal PDGFR-beta drives kidney fibrosis** *EMBO Mol Med.* **12** https://doi.org/10.15252/emmm.201911021

66. Chen HM, Wang L, D'Mello SR (2008) **A chemical compound commonly used to inhibit PKR, 8-(imidazol-4-ylmethylene)-6H-azolidino[5,4-g] benzothiazol-7-one, protects neurons by inhibiting cyclin-dependent kinase** *Eur J Neurosci* **28**:2003–2016 https://doi.org/10.1111/j.1460-9568.2008.06491.x

67. Lopez-Grancha M, Bernardelli P, Moindrot N, et al. (2021) **A Novel Selective PKR Inhibitor Restores Cognitive Deficits and Neurodegeneration in Alzheimer Disease Experimental Models** *J Pharmacol Exp Ther* **378**:262–275 https://doi.org/10.1124/jpet.121.000590

68. Cusack KP, Argiriadi MA, Gordon TD, et al. (2023) **Identification of potent and selective inhibitors of PKR via virtual screening and traditional design** *Bioorg Med Chem Lett.* **79** https://doi.org/10.1016/j.bmcl.2022.129047

Editors

Reviewing Editor

Ilse Daehn

Icahn School of Medicine at Mount Sinai, New York, United States of America

Senior Editor
Diane Harper
University of Michiganâ€Ann Arbor", Ann Arbor, United States of America

Reviewer #1 (Public Review):

Summary:

HIV associated nephropathy (HIVAN) is a rapidly progressing form of kidney disease that manifests secondary to untreated HIV infection and is predominantly seen in individuals of African descent. Tg26 mice carrying an HIV transgene lacking gag and pol exhibit high levels of albuminuria and rapid decline in renal function that recapitulates many features of HIVAN in humans. HIVAN is seen predominantly in individuals carrying two copies of missense variants in the APOL1 gene, and the authors have previously shown that APOL1 risk variant mRNA induces activity of the double strand RNA sensor kinase PKR. Because of the tight association between the APOL1 risk genotype and HIVAN, the authors hypothesized that PKR activation may mediate the renal injury in Tg26 mice, and tested this hypothesis by treating mice with a commonly used PKR inhibitory compound called C16. Treatment with C16 substantially attenuated renal damage in the Tg26 model as measured by urinary albumin/creatinine ratio, urinary NGAL/creatinine ratio and improvement in histology. The authors then performed bulk and single-nucleus RNAseq on kidneys from mice from different treatment groups to identify pathways and patterns of cell injury associated with HIV transgene expression as well as to determine the mechanistic basis for the effect of C16 treatment. They show that proximal tubule nuclei from Tg26 mice appear to have more mitochondrial transcripts which was reversed by C16 treatment and suggest that this may provide evidence of mitochondrial dysfunction in this model. They explore this hypothesis by showing there is a decrease in the expression of nuclear encoded genes and proteins involved in oxidative phosphorylation as well as a decrease in respiratory capacity via functional assessment of respiration in tubule and glomerular preparations from these mouse kidneys. All of these changes were reversed by C16 treatment. The authors propose the existence of a novel injured proximal tubule cell-type characterized by the leak of mitochondrial transcripts into the nucleus (PT-Mito). Analysis of HIV transgene expression showed high level expression in podocytes, consistent with the pronounced albuminuria that characterizes this model and HIVAN, but transcripts were also detected in tubular and endothelial cells. Because of the absence of mitochondrial transcripts in the podocytes, the authors speculate that glomerular mitochondrial dysfunction in this model is driven by damage to glomerular endothelial cells.

Strengths:

The strengths of this study include the comprehensive transcriptional analysis of the Tg26 model, including an evaluation of HIV transgene expression, which has not been previously reported. This data highlights that HIV transcripts are expressed in a subset of podocytes, consistent with the highly proteinuric disease seen in mouse and humans. However, transcripts were also seen in other tubular cells, notably intercalated cells, principal cells and injured proximal tubule cells. Though the podocyte expression makes sense, the relevance of the tubular expression to human disease is still an open question.

The data in support of mitochondrial dysfunction are also robust and rely on combined evidence from downregulation of transcripts involved in oxidative phosphorylation, decreases in complex I and II as determined by immunoblot, and assessments of respiratory capacity in tubular and glomerular preparations. These data are largely consistent with other preclinical renal injury model reported in the literature as well as previous, less thorough assessments in the Tg26 model.

Comments on latest version:

The authors have revised the manuscript to acknowledge the potential limitations of the C16 tool compound used and have performed some additional analyses that suggest the PT-Mito population can be identified in samples from KPMP. The authors added some control images for the in situ hybridizations, which are helpful, though they don't get to the core issue of limited resolution to determine whether mitochondrial RNA is present in the nuclei of injured PT cells. Some additional work has been done to show that C16 treatment results in a decrease in phospho-PKR, a readout of PKR inhibition. These changes strengthen the manuscript by providing some evidence for the translatability of the PT-mito cluster to humans and some evidence for on-target activity for C16. It would be helpful if the authors could quantify the numbers of cells in IHC with nuclear transcripts as well as pointing out some specific examples in the images provided, as comparator data for the snRNAseq studies in which 3-6% of cortex cells had evidence of nuclear mitochondrial transcripts.

https://doi.org/10.7554/eLife.91260.3.sa2

Reviewer #2 (Public Review):

Summary:

Numerous studies by the authors and other groups have demonstrated an important role for HIV gene expression kidney cells in promoting progressive chronic kidney disease, especially HIV associated nephropathy. The authors had previously demonstrated a role for protein kinase R (PKR) in a non-HIV transgenic model of kidney disease (Okamoto, Commun Bio, 2021). In this study, the authors used innovative techniques including bulk and single nuclear RNAseq to demonstrate that mice expressing a replication-incompetent HIV transgene have prominent dysregulation of mitochondrial gene expression and activation of PKR and that treatment of these mice with a small molecule PKR inhibitor ameliorated the kidney disease phenotype in HIV-transgenic mice. They also identified STAT3 as a key upstream regulator of kidney injury in this model, which is consistent with previously published studies. Other important advances include identifying the kidney cell types that express the HIV transgene and have dysregulation of cellular pathways.

Strengths:

Major strengths of the study include the use of a wide variety of state-of-the-art molecular techniques to generate important new data on the pathogenesis of kidney injury in this commonly used model of kidney disease and the identification of PKR as a potential druggable target for the treatment of HIV-induced kidney disease. The authors also identify a potential novel cell type within the kidney characterized by high expression of mitochondrial genes.

Weaknesses:

Though the HIV-transgenic model used in these studies results in a phenotype that is very similar to HIV-associated nephropathy in humans, the model has several limitations that may prevent direct translation to human disease, including the fact that mice lack several genetic factors that are important contributors to HIV and kidney pathogenesis in humans. Additional studies are therefore needed to confirm these findings in human kidney disease.

https://doi.org/10.7554/eLife.91260.3.sa1

Author response:

The following is the authors' response to the previous reviews.

> ***Responses to recommendations for the authors:***
>
> ***Reviewer #1 (Recommendations For The Authors):***
>
> *The manuscript would be strengthened with the following key revisions mostly having to do with image quality:*
>
> *(1) It is very difficult in Figure 4B to see which nuclei actually have evidence of mitochondrial transcripts. It might be helpful to provide arrows to specific cells and also to provide some estimate of the percentage of cells with nuclear mt-transcripts as measured by ISH compared to the 3-6% of cortex cell estimate seen in the snRNAseq analysis.*

As suggested, now we have added arrows to help readers to see the signals in nuclei. The detection threshold of ISH and single-nucleus RNA-seq should be different, and therefore, measuring estimates of PT-Mito by ISH would not be reliable.

> *(2) The phospho-PKR images provided as evidence of C16 activity (Supplemental Figure 1) are too dim to be very useful. Could brighter images be provided?*

We have now adjusted the LUTs of images in Supplemental Figure 1.

https://doi.org/10.7554/eLife.91260.3.sa0